


Electroacupuncture may alleviate neuropathic pain via suppressing P2X7R expression

Molecular Pain
Volume 17: 1–13
© The Author(s) 2021
Article reuse guidelines:
sagepub.com/journals-permissions
DOI: 10.1177/1744806921997654
journals.sagepub.com/home/mpx



Qiaoyun Wu^{1,2}, Jingjing Yue^{1,2}, Li Lin^{1,2}, Xiaolan Yu^{1,2}, Ye Zhou^{1,2},
Xinwang Ying^{1,2}, Xiaolong Chen^{1,2}, Wenzhan Tu^{1,2}, Xinfu Lou²,
Guanhu Yang^{1,2}, Kecheng Zhou^{1,2}, and Songhe Jiang^{1,2} 

Abstract

Neuropathic pain is a severe problem that is difficult to treat clinically. Reducing abnormal remodeling of dendritic spines/synapses and increasing the anti-inflammatory effects in the spinal cord dorsal horn are potential methods to treat this disease. Previous studies have reported that electroacupuncture (EA) could increase the pain threshold after peripheral nerve injury. However, the underlying mechanism is unclear. P2X7 receptors (P2X7R) mediate the activation of microglia and participate in the occurrence and development of neuropathic pain. We hypothesized that the effects of EA on relieving pain may be related to the downregulation of the P2X7R. Spinal nerve ligation (SNL) rats were used as a model in this experiment, and 2'(3')-O-(4-benzoyl)benzoyl ATP (BzATP) was used as a P2X7R agonist. We found that EA treatment decreased dendritic spine density, inhibited synaptic reconstruction and reduced inflammatory response, which is consistent with the decrease in P2X7R expression as well as the improved neurobehavioral performance. In contrast to the beneficial effects of EA, BzATP enhanced abnormal remodeling of dendritic spines/synapses and inflammation. Furthermore, the EA-mediated positive effects were reversed by BzATP, which is consistent with the increased P2X7R expression. These findings indicated that EA improves neuropathic pain by reducing abnormal dendritic spine/synaptic reconstruction and inflammation via suppressing P2X7R expression.

Keywords

Neuropathic pain, electroacupuncture, P2X7R, inflammation, dendritic spine/synaptic reconstruction

Date Received: 29 January 2021; Revised 29 January 2021; accepted: 4 February 2021

Introduction

Neuropathic pain is caused by disease or injury of the somatosensory nervous system. It is a type of chronic pain that is typically characterized by allodynia, hyperalgesia and spontaneous pain.^{1,2} Chronic neuropathic pain lasts for a long time and causes great damage to the body and mental state of patients.³ Due to the complexity of its etiology, currently no method is available to fully alleviate this pain,^{4,5} so research on neuropathic pain is a hot spot in the field of pain.

Peripheral nerve injury can cause the local release of neurotrophic factors, neurotransmitters, chemokines and cytokines. These substances cause neuropathic pain by decreasing the activation threshold of pain receptors.^{6,7} Moreover, damage to nerves can also

cause changes in the internal structure of neurons, further promoting the occurrence and development of pain. Synapses, which are mainly located on dendritic spines,

¹Department of Physical Medicine and Rehabilitation, The Second Affiliated Hospital and Yuying Children's Hospital of Wenzhou Medical University, Wenzhou, China

²Integrative & Optimized Medicine Research Center, China-USA Institute for Acupuncture and Rehabilitation, Wenzhou Medical University, Wenzhou, China

Corresponding Author:

Songhe Jiang, Department of Physical Medicine and Rehabilitation, The Second Affiliated Hospital and Yuying Children's Hospital, China-USA Institute for Acupuncture and Rehabilitation, Wenzhou Medical University, 268 Xue Yuan Xi Road, Wenzhou City 325027, China.

Email: jiangsonghe@wmu.edu.cn



play a very important role in the functional connections between neurons and are key components of information transmission. It has been reported that the synaptic plasticity of spinal dorsal horn neurons changes in spinal nerve ligation (SNL) rats.⁸

Electroacupuncture (EA) is an effective treatment for neuropathic pain that has been applied worldwide given its unique curative effect and limited side effects.⁹ Previous studies have demonstrated that EA can improve neuropathic pain by stimulating IL-10 expression in spinal microglial cells.¹⁰ EA of ST36 and SP6 acupoints can relieve neuropathic pain by reducing IL-6 and IL-1 β expression in spared nerve injury (SNI) rats.¹¹ EA can also improve the synaptic plasticity of brain neurons in rats with nerve injury.^{12,13} Many studies have reported that EA can improve neuropathic pain by anti-inflammatory effects and promoting nerve repair, but the underlying mechanism still needs further exploration.

Microglial cells are activated immediately after nerve injury and are closely related to the generation and development of neuropathic pain.¹⁴ Studies have shown that microglial cells are an important target for analgesia by EA.^{15,16} The P2X7 receptor (P2X7R) is a purinergic receptor expressed on microglial cells. Numerous studies have suggested that P2X7R is associated with pain transmission, neurosensitization, neuronal activation and nerve inflammation.^{17–20} After chronic constriction injury (CCI), the expression of P2X7R increased in the spinal cord and was accompanied by a decrease in the rat pain threshold.²¹ Gene knockout or drug blocking of P2X7R not only significantly reduced tactile pain in neuropathic pain models, but also significantly reduced thermal hyperalgesia.^{20,22,23} In neuropathic pain models, P2X7R overexpression can lead to the activation of microglia and overexpression of TNF- α and IL-1 β .^{24,25} Downregulation of P2X7R with P2X7-specific siRNA prevents the occurrence of long-term potentiation (LTP) and increases the pain threshold.²⁶ Further studies indicated that P2X7R activation promotes the neuroinflammatory response through the p38 MAPK pathway.^{27–29} EA attenuates SNL-induced microglial activation mediated by p38 MAPK.³⁰ Therefore, we hypothesized that the analgesic effect of EA may be achieved by reducing the expression of P2X7R and thus inhibiting the phosphorylation of p38 MAPK.

In this study, we can see that EA contributes to improving neuropathic pain. We used the specific P2X7R agonist 2'(3')-O-(4-benzoyl)benzoyl ATP (BzATP) to identify the role of P2X7R in EA-stimulated neuroprotection and anti-inflammatory effects and further determined the close relationship between EA and P2X7R and their effects on analgesia.

Results

EA increased the pain threshold in SNL rats, whereas BzATP suppressed the EA-induced increase in the pain threshold

The thermal withdrawal latency (TWL) and mechanical withdrawal threshold (MWT) were both measured before the SNL operation and at days 1, 3, 5, 7, 10, 12 and 14 after the SNL operation. As shown in Figure 1(a) and (b), the TWL and MWT of rats decreased significantly after the operation, except in the sham SNL (S) group. On the 14th day after SNL, the scores of the SNL (M) group were lower than those of the S group (TWL, $p < 0.01$; MWT, $p < 0.01$). The scores of the SNL plus EA (M+EA) group were higher than those of the M group (TWL, $p < 0.05$; MWT, $p < 0.01$). The SNL plus BzATP (M+Bz) group had lower scores than the M group (TWL, $p < 0.01$; MWT, $p < 0.01$). The SNL plus EA+BzATP (M+EA+Bz) group had lower scores than the M+EA group (TWL, $p < 0.01$; MWT, $p < 0.01$).

EA reduced the histological changes and neuronal damage in the spinal cord dorsal horn, whereas BzATP exerted the opposite effect

The neuronal morphology was observed by hematoxylin-eosin (HE) staining (Figure 1(c)). No morphological changes were noted in the S group, whereas different degrees of structural failure were observed in other groups. The M group had more swollen cells, disordered neurons and dissolved nuclei than the S group. The M+Bz group had more severe injuries than the M group. Tissue samples from the M+EA group revealed a better performance than those from the M group. The M+EA+Bz group had more swollen cells, disordered neurons and dissolved nuclei than the M+EA group.

The pathological changes were also examined by Nissl staining (Figure 1(d) and (e)). Compared with the S group, less Nissl bodies were observed in the M group ($p < 0.01$). Compared with the M group, the M+EA group showed more Nissl bodies ($p < 0.01$), whereas less Nissl bodies were observed in the M+Bz group ($p < 0.01$). The number of Nissl bodies in the M+EA+Bz group was less than that in the M+EA group ($p < 0.01$).

EA decreased the dendritic spine density after SNL, while BzATP abolished this effect

As shown in Figure 2(c) and (d), the dendritic spine density of the M group was increased compared with that of the S group ($p < 0.01$), whereas EA decreased the spine density in the M+EA group ($p < 0.01$). The M+Bz group had more dendritic spines than the M group

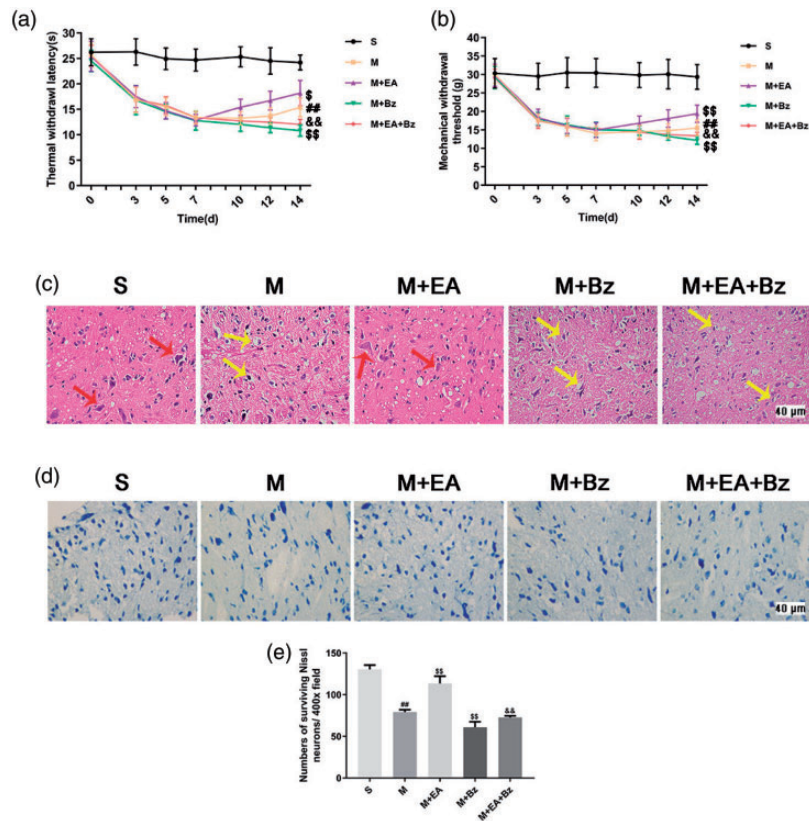


Figure 1. EA increased the threshold of pain, reduced the damage of tissue structure and promoted the recovery of neuron function, whereas BzATP blocked these effects. (a) Thermal withdrawal latency (TWL). (n = 15). (b) Mechanical withdrawal threshold (MWT). (n = 15). (c) HE staining (lamina I-IV). Scale bars, 40 μ m. The red arrows show normal neurons, and the yellow arrows show cells with somatic dissolution and nucleus shrinkage, accompanied by the formation of voids in surrounding tissues. (d) Nissl staining in each group (lamina I-IV). (n = 4). Scale bars, 40 μ m. (e) Numbers of surviving Nissl neurons per 400x field. (n = 4). Columns represent the mean \pm SD. ### p < 0.01 vs. the S group; \$\$ p < 0.01 vs. the M group; && p < 0.01 vs. the M+EA group.

(p < 0.05). The dendritic spine density of the M+EA+Bz group was greater than that of the M+EA group (p < 0.01).

EA improved the synaptic plasticity of spinal dorsal horn neurons after SNL, whereas BzATP had the opposite effect

The changes in the synapses of each group were examined by transmission electron microscopy (Figure 2(e) to (h)). The M group had more abnormal synapses (p < 0.05) with smaller synaptic space (p < 0.01) and more synaptic vesicles (p < 0.01) than the S group. The M+EA group had fewer abnormal synapses (p < 0.05) with larger synaptic space (p < 0.01) and fewer synaptic vesicles (p < 0.01) than the M group. The synapses of the M+EA group appeared to have larger synaptic space (p < 0.01) and fewer synaptic vesicles (p < 0.01) compared with the M+EA+Bz group.

EA decreased expression of proinflammatory factors and promoted expression of anti-inflammatory mediators, whereas BzATP played the opposite role

Western blot (Figure 3(a) to (e)) showed that the M group exhibited increased IL-1 β , IL-6, TNF- α and IL-10 expression compared with the S group (IL-1 β , p < 0.01; IL-6, p < 0.01; TNF- α , p < 0.01; IL-10, p < 0.01), whereas EA decreased IL-1 β , IL-6, and TNF- α expression and increased IL-10 expression in SNL rats (IL-1 β , p < 0.01; IL-6, p < 0.01; TNF- α , p < 0.05; IL-10, p < 0.01). The M+Bz group exhibited increased IL-1 β , IL-6, and TNF- α expression and lower IL-10 expression (IL-1 β , p < 0.01; IL-6, p < 0.01; TNF- α , p < 0.05; IL-10, p < 0.01) compared with the M group. The M+EA+Bz group exhibited increased IL-1 β , IL-6, and TNF- α expression and reduced IL-10 expression compared with the M+EA group (IL-1 β , p < 0.01; IL-6, p < 0.01; TNF- α , p < 0.01; IL-10, p < 0.01). Additionally, changes in IL-1 β , IL-6, TNF- α and IL-10

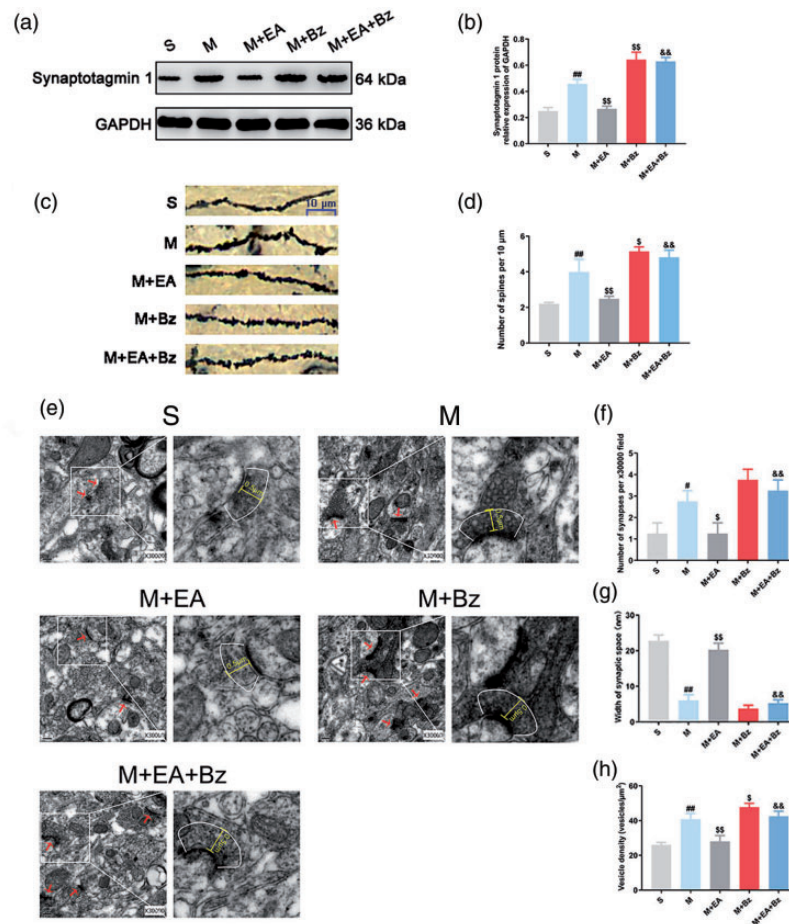


Figure 2. EA reduced abnormal remodeling of dendritic spines/synapses, whereas BzATP had the opposite effects. (a) and (b) Representative Western blots and quantification data of the expression of Synaptotagmin 1/GAPDH. ($n = 3$). (c) Dendritic spines. Scale bars, $10 \mu\text{m}$. (d) Number of spines per $10 \mu\text{m}$. ($n = 3$). (e) The ultrastructure of synapses in the spinal dorsal horn from rats in each group ($0.2 \mu\text{m}$, $30,000\times$). (f) Number of synapses per $30000\times$ field. ($n = 4$). (g) Width of synaptic space (nm). ($n = 4$). (h) Vesicle density (vesicles/ μm^2). ($n = 4$). Columns represent the mean \pm SD. $\#p < 0.05$ and $\#\#\#p < 0.01$ vs. the S group; $\$p < 0.05$ and $\$\$\$p < 0.01$ vs. the M group; $\&\&p < 0.01$ vs. the M+EA group.

expression in each group examined by qPCR (Figure 3(f) to (i)) and enzyme-linked immunosorbent assay (ELISA) (Figure 3(j) to (m)) were consistent with the trends in protein expression levels.

EA decreased SNL-induced overexpression of synaptotagmin 1, BDNF and Iba1, whereas BzATP prevented this effect

Western blot (Figure 2(a) and (b); Figure 4(a) and (b); Figure 5(a) and (b)) showed that the M group had higher expression of Synaptotagmin 1, BDNF and Iba1 than the S group (Synaptotagmin 1, $p < 0.01$; BDNF, $p < 0.01$; Iba1, $p < 0.01$). The M+EA group exhibited lower Synaptotagmin 1, BDNF and Iba1 expression levels compared with the M group (Synaptotagmin 1, $p < 0.01$; BDNF, $p < 0.01$; Iba1, $p < 0.05$), whereas the M+Bz group had higher Synaptotagmin 1, BDNF and

Iba1 expression levels compared with the M group (Synaptotagmin 1, $p < 0.01$; BDNF, $p < 0.01$; Iba1, $p < 0.05$). BzATP administration increased Synaptotagmin 1, BDNF and Iba1 protein levels in the M+EA+Bz group compared with the M+EA group (Synaptotagmin 1, $p < 0.01$; BDNF, $p < 0.01$; Iba1, $p < 0.01$).

Regarding immunofluorescence (Figure 4(c) to (e); Figure 5(c) and (d)), the M group exhibited more BDNF- and Iba1-positive cells in the laminae I–II and laminae III–IV regions than the S group (BDNF, laminae I–II/laminae III–IV, $p < 0.01/p < 0.01$; Iba1, laminae I–II/laminae III–IV, $p < 0.01/p < 0.01$). The M+EA group had fewer positive cells than the M group (BDNF, laminae I–II/laminae III–IV, $p < 0.01/p < 0.01$; Iba1, laminae I–II/laminae III–IV, $p < 0.01/p < 0.01$). More positive cells were observed in the M+Bz group compared with the M group (BDNF, laminae I–II/

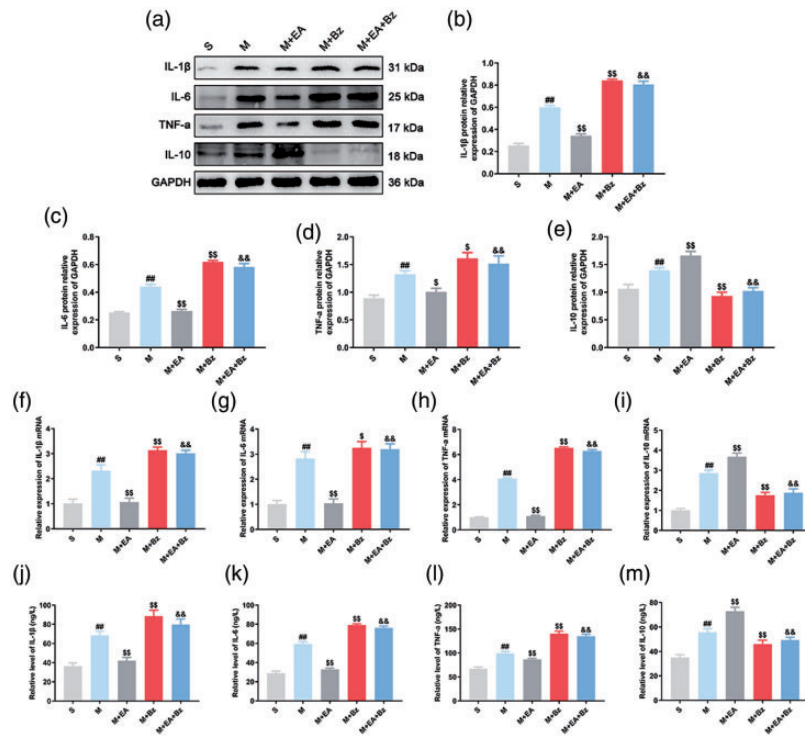


Figure 3. EA decreased expression of IL-1 β , IL-6, and TNF- α and increased expression of IL-10 after SNL, while BzATP had the opposite effects. (a) to (e) Representative Western blots and quantification data of the expression of IL-1 β /GAPDH, IL-6/GAPDH, TNF- α /GAPDH and IL-10/GAPDH in each group. (n = 3). (f) to (i) qPCR showing the expression of IL-1 β , IL-6, TNF- α and IL-10 mRNA in the spinal cord. (n = 6). (j) to (m) The content of IL-1 β , IL-6, TNF- α and IL-10 in the rat serum measured by ELISA. (n = 6). Columns represent the mean \pm SD. ###*p* < 0.01 vs. the S group; \$*p* < 0.05 and \$\$*p* < 0.01 vs. the M group; &&*p* < 0.01 vs. the M+EA group.

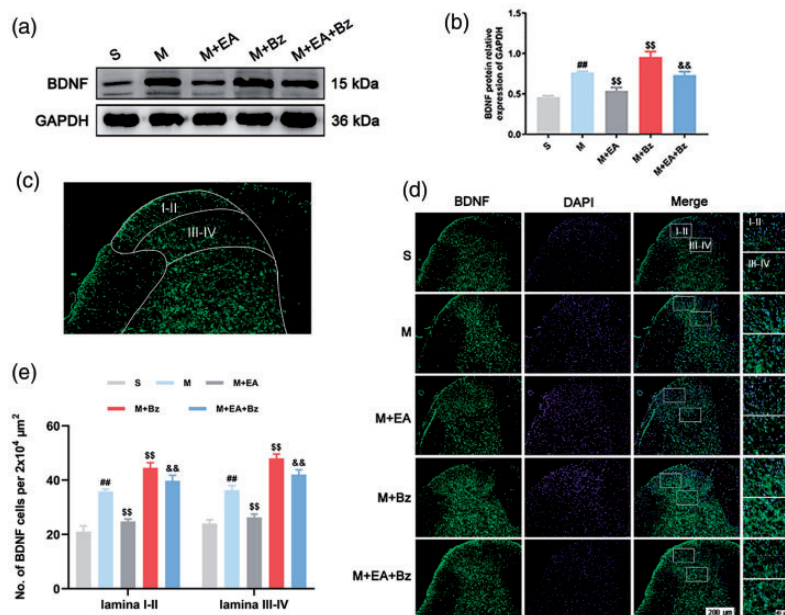


Figure 4. EA decreased the expression levels of BDNF, while BzATP reversed this effect. (a) and (b) Protein expression levels of BDNF in the spinal cord and quantification data of the expression of BDNF/GAPDH in each group. (n = 3). (c) A representative image at low magnification shows the observed spinal cord site (lamina I-II and lamina III-IV). (d) Immunofluorescence of BDNF-positive cells in the spinal dorsal horn. Scale bars, 200 μ m; 40 μ m. (e) Number of BDNF-positive cells per 2x10⁴ μ m² in the spinal dorsal horn (lamina I-II and lamina III-IV). (n = 4). Columns represent the mean \pm SD. ###*p* < 0.01 vs. the S group; \$*p* < 0.05 and \$\$*p* < 0.01 vs. the M group; &&*p* < 0.01 vs. the M+EA group.

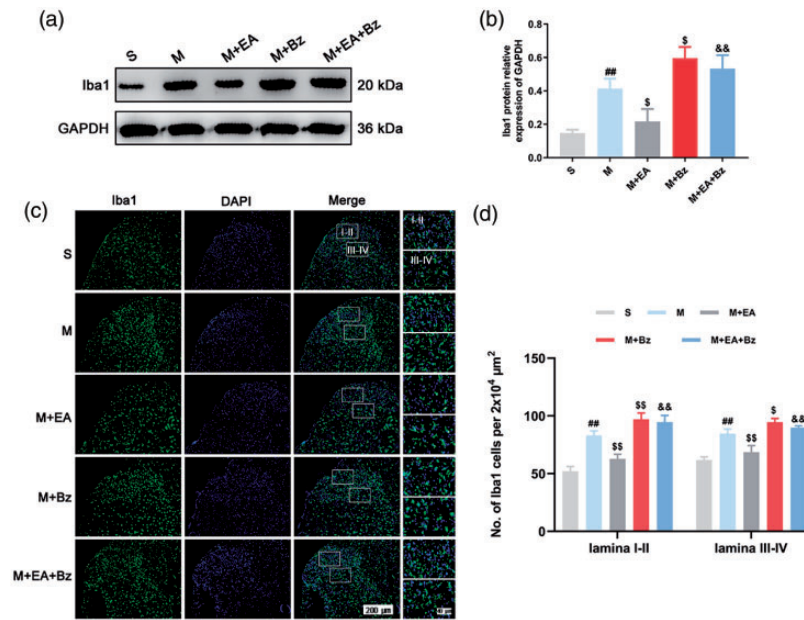


Figure 5. EA decreased the expression levels of Iba1, while BzATP reversed this effect. (a) and (b) Protein expression levels of Iba1 in the spinal cord and quantification data of the expression of Iba1/GAPDH in each group. ($n = 3$). (c) Immunofluorescence of Iba1-positive cells in the spinal dorsal horn. Scale bars, 200 μm ; 40 μm . (d) Number of Iba1-positive cells per $2 \times 10^4 \mu\text{m}^2$ in the spinal dorsal horn (lamina I-II and lamina III-IV). ($n = 4$). Columns represent the mean \pm SD. ### $p < 0.01$ vs. the S group; \$ $p < 0.05$ and \$\$ $p < 0.01$ vs. the M group; && $p < 0.01$ vs. the M+EA group.

laminae III–IV, $p < 0.01/p < 0.01$; Iba1, laminae I–II/laminae III–IV, $p < 0.01/p < 0.05$). The M+EA+Bz group had more positive cells than the M+EA group (BDNF, laminae I–II/laminae III–IV, $p < 0.01/p < 0.01$; Iba1, laminae I–II/laminae III–IV, $p < 0.01/p < 0.01$).

EA downregulated P2X7R and p-p38 expression following SNL, whereas BzATP played the opposite role

P2X7R, p38 and p-p38 protein expression levels were examined by Western blot (Figure 6(a) to (c)). No significant differences in p38 expression levels were noted in any of the groups ($p > 0.05$). The M group had higher levels of P2X7R and p-p38/p38 than the S group (P2X7R, $p < 0.01$; p-p38/p38, $p < 0.01$). The M+EA group had lower P2X7R and p-p38/p38 expression levels than the M group (P2X7R, $p < 0.01$; p-p38/p38, $p < 0.01$), whereas the M+Bz group had higher P2X7R and p-p38/p38 expression levels than the M group (P2X7R, $p < 0.01$; p-p38/p38, $p < 0.01$). P2X7R and p-p38/p38 levels in the M+EA+Bz group were higher than those in the M+EA group (P2X7R, $p < 0.01$; p-p38/p38, $p < 0.01$).

In terms of immunofluorescence (Figure 6(d) to (g)), the M group exhibited more P2X7R- and p-p38-positive cells in the laminae I–II and laminae III–IV regions of the spinal dorsal horn than the S group (P2X7R, laminae I–II/laminae III–IV, $p < 0.01/p < 0.01$; p-p38,

laminae I–II/laminae III–IV, $p < 0.01/p < 0.01$). The M+EA group had a lower number of P2X7R- and p-p38-positive cells than the M group (P2X7R, laminae I–II/laminae III–IV, $p < 0.01/p < 0.01$; p-p38, laminae I–II/laminae III–IV, $p < 0.01/p < 0.01$). The number of P2X7R- and p-p38-positive cells in the M+Bz group was increased compared with those in the M group (P2X7R, laminae I–II/laminae III–IV, $p < 0.01/p < 0.01$; p-p38, laminae I–II/laminae III–IV, $p < 0.01/p < 0.01$). The M+EA+Bz group had more positive cells than the M+EA group (P2X7R, laminae I–II/laminae III–IV, $p < 0.01/p < 0.01$; p-p38, laminae I–II/laminae III–IV, $p < 0.01/p < 0.01$).

Discussion

The current study indicated that EA contributes to reducing abnormal remodeling of dendritic spines/synapses and regulating the expression of inflammatory factors via suppressing P2X7R expression.

The spinal cord dorsal horn is an important site for the body to modulate or integrate injurious information. This site exhibits a large amount and distribution of neuroactive substances and receptors and is one of the main distribution areas of pain, touch and temperature neurons.³¹ The study of pain-related regulatory factors in the spinal cord dorsal horn is helpful to understand the mechanism of neuropathic pain occurrence and maintenance. Studies have shown that one of the

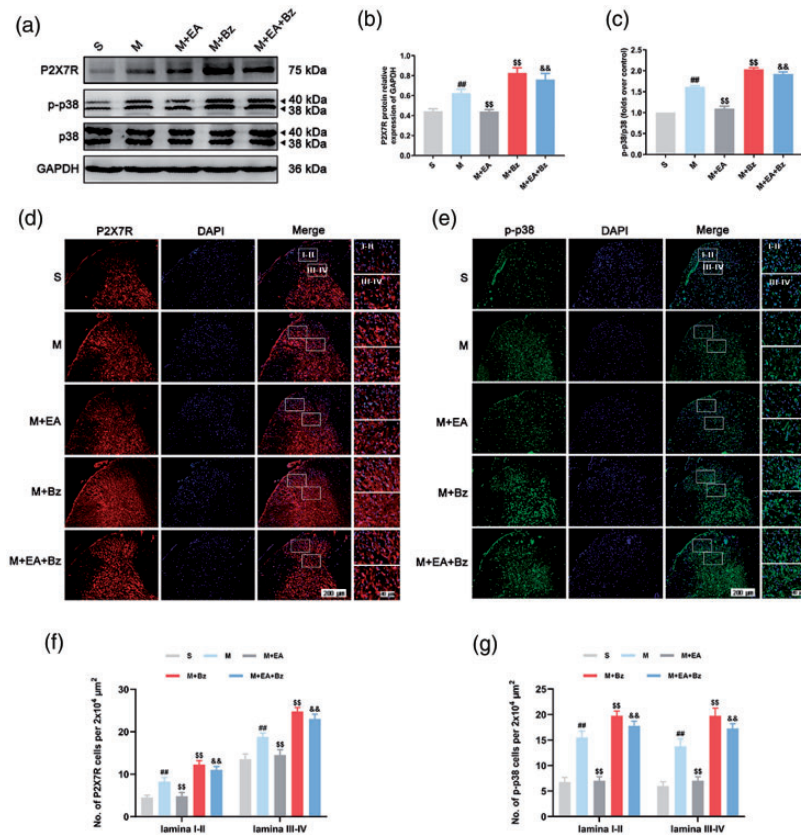


Figure 6. EA decreased the expression of P2X7R and p-p38 in the spinal dorsal horn after SNL, while BzATP reversed this effect. (a) to (c) Representative Western blots and quantification data of the expression of P2X7R/GAPDH, p-p38/p38 in each group. (n = 3). (d) and (e) Immunofluorescence of P2X7R- and p-p38-positive cells in the spinal dorsal horn. Scale bars, 200 μm ; 40 μm . (f) and (g) Number of P2X7R- and p-p38-positive cells per $2 \times 10^4 \mu\text{m}^2$ in the spinal dorsal horn (lamina I-II and lamina III-IV). Columns represent the mean \pm SD. (n = 4). ## $p < 0.01$ vs. the S group; \$\$ $p < 0.01$ vs. the M group; && $p < 0.01$ vs. the M+EA group.

mechanisms of neuropathic pain is the central sensitization of spinal dorsal horn neurons, which primarily manifests as the LTP of synaptic transmission.³² The synapse is the site where neurons connect and is also the component of information transmission. Neurotransmitters stored and released by presynaptic vesicles transmit information to the postsynaptic membrane through synaptic space. Numerous neurotransmitter-degrading enzymes are present in the synaptic space. The wider the synaptic gap is, the longer the transmission time of neurotransmitters, and the more degraded the neurotransmitters. Therefore, the increase of the number of synapses, synaptic vesicle density and the narrowing of synaptic space may be the structural basis for the enhancement of synaptic transmission function. In this study, we found that the dendritic spine density increased after SNL, and more synapses, more synaptic vesicles and smaller synaptic gaps were observed in the M group compared with the S group. These changes in the number and structure of dendritic spines and synapses may lead to an increase in abnormal signaling, thus resulting in an increase in allergic pain. Furthermore, the

M group exhibited increased IL-1 β , IL-6, and TNF- α expression levels compared with the S group, indicating that the occurrence of neuropathic pain is partly caused by the release of proinflammatory factors.

Many studies have reported that EA plays an important role in the treatment of neuropathic pain. EA at the ST 41-LR 3 and KI 3-1 acupoints helped relieve the pain caused by fiber neuropathy.³³ EA can reduce pain by inhibiting the activation of glial cells in rats injected with the chemotherapeutic drug paclitaxel.³⁴ The application of EA also inhibited IL-1 β and IL-6 expression and promoted IL-10 activity.¹¹ Synaptotagmin 1, the main Ca²⁺ sensor in the process of neurotransmitter release mediated by synaptic vesicles, is increased in SNI rats, whereas the application of EA decreased its expression and increased the pain threshold.³⁵ Acupuncture has the feedback regulation effect of multiple afferent pathways (clinical acupuncture feedback law and multi-law acupoint matching). ST-36 and BL-60 are commonly used therapeutic points for lower limb pain,^{36,37} and low-frequency (2 Hz) electrical stimulation plays a beneficial role in analgesia.^{38,39} In our study, EA

at ST-36 and BL-60 increased the MWT and TWL of SNL rats, and the structure of the spinal dorsal horn was also improved. The expression levels of proinflammatory factors in the M+EA group were reduced compared with the M group, whereas IL-10 expression increased in the M+EA group compared with that in the M group. Furthermore, EA treatment inhibited the abnormal remodeling of dendritic spines/synapses induced by SNL. These findings indicated that the analgesic effect of EA may be related to the inhibition of inflammatory factors and dendritic spine/synaptic remodeling. However, the underlying mechanism requires further exploration.

Many previous studies have shown that the activation of microglial cells is a key factor in the generation and persistence of neuropathic pain.^{34,40} Adenosine triphosphate (ATP) is a transmitter involved in the modulation of traumatic information in the spinal cord. The damaged tissue cells and sensory nerve endings can release a large amount of ATP after peripheral nerve injury.^{41,42} Studies have shown that ATP activates microglial cells, induces microglial cell aggregation and proliferation, and promotes the release of a variety of proinflammatory factors and neuroactive substances.⁴³⁻⁴⁵ The release of proinflammatory factors and neuroactive substances can lead to the enhancement of excitatory synaptic transmission and hyperactivity of dorsal horn neurons (central sensitization). The expression of microglial brain-derived neurotrophic factor (BDNF) is increased in SNI rats,⁴⁴ thus enhancing synaptic plasticity.⁴⁶ P2X7R is a purinergic receptor expressed on microglial cells and studies have shown P2X7R expression is increased in rats with peripheral nerve injury.^{21,26} The antagonist of P2X7R (A804598) decreased p38 phosphorylation, glial activation and IL-1 β expression, which is consistent with less nerve damage and better neuronal survival.⁴⁷ EA attenuates SNL-induced microglial activation mediated by p38 MAPK.³⁰ Thus, we hypothesized that the changes in the expression of inflammatory factors and the morphology and structure of dendritic spine/synapses in SNL rats might be related to the regulation of P2X7R and p38 MAPK. In our study, we found that BzATP aggravated spinal dorsal horn neuron injury and promoted the expression of P2X7R, p-p38, Synaptotagmin 1, Iba1, BDNF and proinflammatory factors in SNL rats, indicating that P2X7R may mediate the occurrence of neuropathic pain. Furthermore, the increased expression of BDNF, Synaptotagmin 1 and proinflammatory factors may lead to abnormal increase of dendritic spines and excessive release of synaptic vesicles, which results in the enhancement of abnormal signal transmission and further pain development. Immunofluorescence results showed that BzATP promoted the expression of P2X7R, p-p38, BDNF and Iba1 in lamina I-II and lamina III-IV in

the spinal dorsal horn after SNL. Because primary afferent A-fibers and C-fibers terminate and synapse with second-order neurons in the lamina I-II and lamina III-IV regions,⁴⁸ the present results suggest that the activation of P2X7R induced by SNL may play a key role in the dorsal horn transmission of nociceptive signals.

The relationship between EA and P2X7R was also analyzed in this study. The P2X7R agonist BzATP inhibited the neuropathic pain improvement effects of EA. Results in this study suggest that EA inhibits dendritic spine/synaptic remodeling and regulates the expression of inflammatory factors through inhibiting the expression of P2X7R. Furthermore, previous studies have shown that the central mechanism of EA against hyperalgesia may be related to the decreased expression of p-p38 MAPK, which subsequently reduces microglial activation in neuropathic pain.³⁰ Therefore, we hypothesize that EA may inhibit the phosphorylation of p38 by inhibiting the activity of P2X7R in microglia to reduce inflammation and inhibit the abnormal synaptic remodeling of neurons.

Some limitations also exist in this study. First, although we examined P2X7R-positive cells based on immunofluorescence staining, we did not perform double staining for P2X7R and Iba1 in rat spinal dorsal horn sections. Second, we can not demonstrate that the analgesic effect of EA is mediated by the inhibition of p38 phosphorylation in microglia, and this notion needs to be further explored in subsequent experiments. Third, according to the present study, we can only assume that the analgesic effect of EA by reducing P2X7R expression is one possibility. It is better to use P2X7R inhibitor or P2X7R siRNA to further prove this mechanism.

In conclusion, the present study indicates that EA may improve neuropathic pain by reducing abnormal dendritic spine/synaptic reconstruction and inflammation via P2X7R downregulation (Figure 7) and P2X7R can be used as a potential clinical therapeutic target for neuropathic pain.

Materials and methods

Antibodies and reagents

The anti-P2X7R antibody was obtained from Santa Cruz Biotechnology (Dallas, TX, USA). Anti-p38, anti-p-p38, anti-IL-1 β , anti-IL-6, anti-TNF- α , anti-IL-10 and anti-Synaptotagmin 1 antibodies were obtained from Affinity Biosciences (Cincinnati, OH, USA). The anti-Iba1 antibody was obtained from Wako (Wako Pure Chemical Industries, Ltd). An anti-GAPDH was obtained from Bioworld. The anti-BDNF antibody and the P2X7R-specific agonist BzATP were obtained from Abcam (Cambridge Science Park, Cambridge,

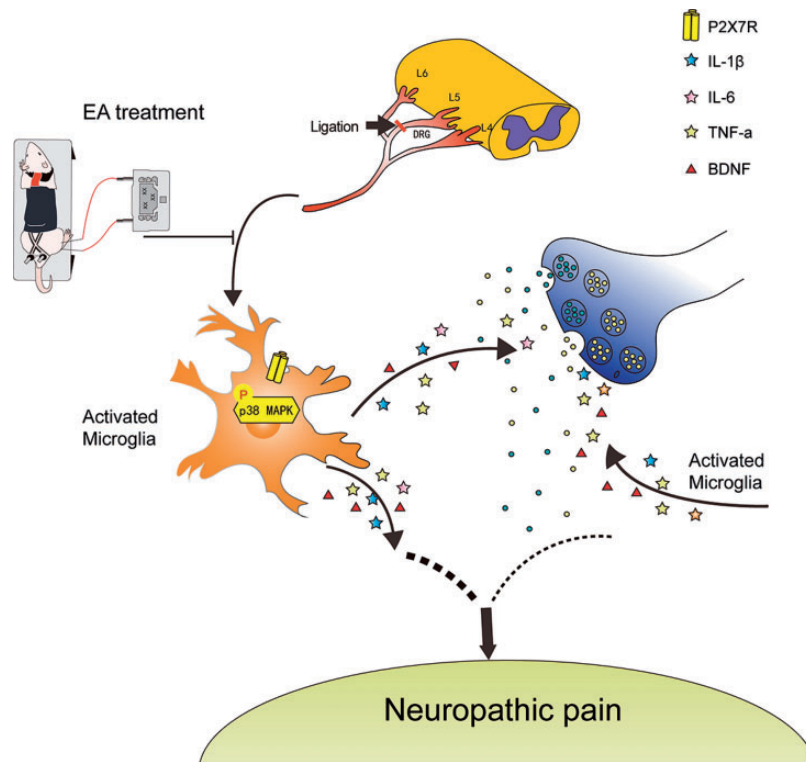


Figure 7. Possible pathway for the analgesic effect of EA after SNL injury. After L5 spinal nerve injury, the expression of P2X7R in microglia of spinal dorsal horn increased, which promoted the phosphorylation of p38. p38 phosphorylation may activate microglia, thus promoting the release of inflammatory factors and BDNF, leading to the enhancement of synaptic signal transmission and the hyperactivity of neurons in the spinal dorsal horn. These processes promote the occurrence of neuropathic pain. EA alleviated neuropathic pain by inhibiting P2X7R activity.

UK). An FD Rapid GolgiStain Kit was obtained from FD Neurotechnologies, Inc. (Guilford, MD, USA).

Animals

Adult male Sprague-Dawley rats (200–250 g) were provided by the Laboratory Animal Center of Wenzhou Medical University. All experiments were approved by the Animal Research Committee of Wenzhou Medical University and followed the National Institutes of Health Guide for the Care and Use of Laboratory Animals. The rats lived in a room where day and night alternated regularly and the temperature was maintained at 22–24°C. The rats drank and ate freely. There are five groups in this study: sham SNL group (S group), SNL group (M group), SNL plus EA group (M+EA group), SNL plus BzATP group (M+Bz group) and SNL plus EA+Bz group (M+EA+Bz group). Rats were sacrificed on the 14th day after SNL and the spinal dorsal horn was collected as a tissue sample. The rats were deeply anesthetized with isoflurane. After 10 minutes of anesthesia, the rats were confirmed to have no response to clipping the tail and claws using forceps, and the samples of the rats were collected.

Spinal nerve ligation

After anesthesia with 2% sodium pentobarbital (30 mg/kg, i.p.), the rats were placed in the prone position, and the skin and muscles of the rats' backs were cut open to remove the L5 transverse process and expose the L5 spinal nerves. The L5 spinal nerves were ligated with 4–0 silk thread. The L5 spinal nerves of rats in the S group were exposed for 3 minutes without ligation.⁴¹

EA stimulation and injection of BzATP

ST-36 and BL-60 were chosen as EA points in this study. The ST-36 acupoint is 5 mm lateral to the anterior tubercle of the tibia. The BL-60 acupoint is located in the depression between the end of the lateral malleolus and the Achilles tendon. Rats in the M+EA and M+EA+Bz groups received EA treatment every 24 hours from the 7th day after SNL operation, lasting for 7 days. EA was performed between 08:00–10:00 every day. The rats were fixed in the fixed device designed by our laboratory (patent application no. 201110021482.5; State Intellectual Property Office), without anesthesia, and the rats could receive EA treatment comfortably. Acupuncture needles were inserted for 2–3 mm and

stimulated (2 Hz, 1.5 mA) for 30 min with an electric stimulation device (Hans-200e, Jisheng Medical Device). The rats in the M+Bz and M+EA+Bz groups were intrathecally administered BzATP (0.5 µg/rat)⁴⁹ dissolved in saline (10 µL/rat) 30 min before EA treatment. Rats in the S, M and M+EA groups were injected with the same volume of saline (10 µL/rat).

Mechanical withdrawal threshold

The behavioral tests were conducted at 12:00–15:00 using a 2392 electronic von Frey anesthesiometer (IITC Life Sciences, California, USA). Rats were placed in the instrument to adjust for 20 min and then subject to a series of increasing von Frey stimuli ranging from 0 to 60 g at the plantar surface. As the paw twitched, the value displayed on the instrument was recorded. The test was conducted every 5 min for a total of 5 rounds of testing. The average of these values in each group were considered the MWT threshold.

Thermal withdrawal latency

TWL was assessed with an A37370 plantar tester (Ugo Basilee, Milan, Italy). The rats were placed into the instrument to acclimate for 30 min before the test began. Radiant heat was set at 60°C, and the affected side foot of the rats was placed in a radiant heat source. Radiant heat was irradiated to the plantar floor through a glass plate. When the rats lifted their paws in pain, the beam shut off. The test was conducted every 5 min for a total of 5 rounds of testing. The average of these values in each group was considered the MWT threshold.

Golgi staining and measurement of dendritic spine density

An FD Rapid GolgiStain Kit (Guilford, MD, USA) was used for Golgi staining. L4-6 spinal cord segments were stored in a mixed solution of A and B (A: B = 1:1) for 2 weeks out of light. The specimen was then placed in solution C and kept in darkness for 48 hours. The samples were then cut into 150 µm thick slices and attached to the slide. Then the sections were stained in strict accordance with the instructions. The dyeing process was as follows: the slices were placed in a mixture solution of D, E and distilled water (D: E: distilled water = 1:1:2) for 10 minutes, then washed with distilled water, and then re-dyed with crystal violet solution. Finally, the slices were dehydrated with alcohol, transparent with xylene, and sealed with gum sealant. Dendritic spine density was expressed as the number of dendritic spines per 10 µm segment of dendrite.⁵⁰

Western blot

The L4-6 segments of the spinal cord were collected and homogenized in RIPA protein lysis buffer (PMSF: RIPA = 1:100). The samples were centrifuged at 4°C at 15,000×g for 5 min and the supernatant was collected. The sample concentration was measured with a BCA protein detection kit (Beyotime Corp, China). Equivalent (85 µg) amounts of proteins were subjected to Tris-HCl SDS-PAGE gel (Bio-Rad Laboratories, CA, USA) electrophoresis for 1.5 h at 80 V. Proteins were then transferred to PVDF membranes (Millipore Corp, MA, USA) with a 300 mA current. The membranes were blocked in 5% skim milk for 2–3 hours. The membrane was then incubated in diluted primary antibodies at 4°C for 16 hours. The primary antibodies are as follows: mouse anti-P2X7R (1:500, sc-514962); rabbit anti-p38 (1:500, AF6456); rabbit anti-phospho-p38 MAPK (1:500, AF4001); rabbit anti-BDNF (1:1,000, ab108319); rabbit anti-Iba1 (1:200, 019–19741); rabbit anti-Synaptotagmin 1 (1:500, DF6174); and rabbit anti-GAPDH (1:5,000, AP0063). Then, the membranes were placed in diluted secondary antibodies for 1.5–2 hours. An enhanced chemiluminescence (ECL) kit (Beyotime Corp, China) was used to detect the bands. The quantity of band intensity was analyzed using AlphaEaseFC (version 4.0).

Quantitative real-time PCR

The tissues were isolated by TRIzol (Invitrogen, USA). A LightCycler 480 (Roche, USA) and SYBR Green Supermix (QPK-212, Tokyo, Japan) were used to conduct real-time amplification. The PCR conditions were as follows: inactivation at 95°C for 5 min, denaturation at 95°C for 10 s, primer annealing at 60°C for 10 s, and then elongation at 72°C for 10 s. The sequences of the primers were as follows (5′-3′): IL-1β, sense ATCTCACAGCAGCATCTCGACAAG, antisense CACACTAGCAGGTCGTCATCATCC; IL-6, sense ACTTCCAGCCAGTTGCCTTCTTG, antisense TGG TCTGTTGTGGGTGGTATCCTC; TNF-α, sense AAAGGACACCATGAGCACGGAAAG, antisense CGCCACGAGCAGGAATGAGAAG; IL-10, sense CTGCTCTTACTGGCTGGAGTGAAG, antisense TGGGTCTGGCTGACTGGGAAG; and ACTB (beta-actin), sense TGTCACCAACTGGGACGATA, antisense GGGGTGTTGAAGGTCTCAA. Relative expression was analyzed by the 2^{-ΔΔCt} method.⁵¹

Immunofluorescence

After the treatment, the rats were perfused with normal saline and 4% paraformaldehyde. L4-6 spinal cords were collected and placed in paraformaldehyde for 24 hours. The tissues were paraffin-embedded after fixation. The

sample was then dewaxed with xylene and hydrated in ethanol. The slices were incubated with 3% H₂O₂ for 12 min and then blocked with 10% goat serum for 1 hour. The sections were placed in the diluted primary antibody for 16 hours at 4°C. Then, the slices were washed and incubated with diluted secondary antibodies for 1 hour. Then, 4',6-diamidino-2-phenylindole (DAPI) was added to the slices for 10 min and imaged using a fluorescence microscope (Olympus, Tokyo, Japan).

He staining

The removed tissues (L4-6) were embedded in paraffin, and tissues were cut into sections. The sections were then dewaxed twice with xylene (five min every time) and rehydrated with gradient ethanol for 1 min. Then samples were stained with hematoxylin for 2 min, separated with 1% hydrochloric acid ethanol for 10 s and stained with eosin for 1 min. Then, tissues were dehydrated by 95% and 100% ethanol twice (1 min every time). Finally, sections were mounted using neutral balsam.

Nissl staining

On the 14th day after SNL, the animals were anesthetized, and the L4-6 spinal cords were collected and fixed with 4% paraformaldehyde for 24 hours. The tissues were embedded in paraffin. Then, the tissues were cut into 4-micron slices and attached to the slides. The tissues were stained with 0.5% thionine for 10 min, and then the slices were dehydrated by an ethanol gradient. Finally, the tissues were soaked in xylene for 5 min. The quantitative data of Nissl staining were shown as numbers of surviving Nissl neurons per 400 x field in each spinal cord section.

Transmission electron microscopy

On the 14th day after the operation, the L4-6 spinal cords were quickly removed after anesthesia, and the dorsal horn of the spinal cord was cut into several 1 × 1 × 2 segments. The tissues were fixed in glutaraldehyde for 24 hours. The tissues were removed and fixed with osmic acid for 1 hour and then stained with uranium acetate for 2 hours. The tissues were dehydrated with acetone and embedded. The embedded mass was subject to coronal sectioning and stained with toluidine blue. The synaptic structures were observed by Hitachi transmission electron microscopy. Image J software was used to determine the width of synaptic space and the density of synaptic vesicles. The synaptic space is not an absolutely uniform structure of equal width, so the multi-value averaging method is used to reduce the error. In this experiment, each synapse was measured five times, and the average value was taken as the measurement value of synaptic gap. The density of synaptic vesicles

was expressed by the ratio of the number of synaptic vesicles in the range of 0.5 μm from the presynaptic membrane (range of white box) to the area of the corresponding white box.

Elisa

Rat serum was collected, and the kits (Shanghai Boyun Biotech Co., Ltd) were used to test the contents of IL-1β, IL-6, TNF-α and IL-10 according to the instructions.

Statistical analysis

Data were analyzed with SPSS 23.0 statistical software and are shown as the mean ± SD. Two-way ANOVA followed by Tukey's post hoc test was used to analysis the change of TWL and MWT. One-factor analysis of variance (ANOVA) was used among the multiple groups to examine other statistical significance and Dunnett's T3 method was use for post hoc comparisons. $p < 0.05$ was considered statistically significant.

Acknowledgments

We thank Wenzhou Medical University for its abundant research platform.

Author Contributions

Wu Qiaoyun, Zhou Kecheng and Jiang Songhe: Conceptualization; Wu Qiaoyun and Yue Jingjing: Data curation; Tu Wenzhan, Lou Xinfa and Yang Guanhu: Formal analysis; Wu Qiaoyun, Ying Xinwang, Zhou Ye and Chen Xiaolong: Methodology; Wu Qiaoyun, Yu Xiaolan and Lin Li: Validation; Wu Qiaoyun and Zhou Kecheng: Writing—original draft; Wu Qiaoyun, Zhou Kecheng and Jiang Songhe: Writing—review & editing.

Declaration of Conflicting Interests

The author(s) declared no potential conflicts of interest with respect to the research, authorship, and/or publication of this article.

Funding

The author(s) disclosed receipt of the following financial support for the research, authorship, and/or publication of this article: This work was supported by the National Natural Science Foundation of China (grant number 81873376, 81574074); the Basic Research Program of Wenzhou City (Y20190192).

ORCID iD

Songhe Jiang  <https://orcid.org/0000-0002-4778-8187>

References

1. Xun S, Zheng R. Dexmedetomidine alleviates neuropathic pain by regulating JAK/STAT pathway in rats. *J Cell Biochem* 2020; 121: 2277–2283.

2. Finnerup NB, Haroutounian S, Kamerman P, Baron R, Bennett DL, Bouhassira D, Cruccu G, Freeman R, Hansson P, Nurmikko T, Raja SN, Rice AS, Serra J, Smith BH, Treede RD, Jensen TS. Neuropathic pain: an updated grading system for research and clinical practice. *Pain* 2016; 157: 1599–1606.
3. Zou Y, Cao Y, Liu Y, Zhang X, Li J, Xiong Y. The role of dorsal root ganglia PIM1 in peripheral nerve injury-induced neuropathic pain. *Neurosci Lett* 2019; 709: 134375.
4. Yu H, Zhang P, Chen YR, Wang YJ, Lin XY, Li XY, Chen G. Temporal changes of spinal transcriptomic profiles in mice with spinal nerve ligation. *Front Neurosci* 2019; 13: 1357.
5. Xu H, Dang SJ, Cui YY, Wu ZY, Zhang JF, Mei XP, Feng YP, Li YQ. Systemic injection of thalidomide prevent and attenuate neuropathic pain and alleviate neuroinflammatory response in the spinal dorsal horn. *JPR* 2019; 12: 3221–3230.
6. Iyengar S, Ossipov MH, Johnson KW. The role of calcitonin gene-related peptide in peripheral and central pain mechanisms including migraine. *Pain* 2017; 158: 543–559.
7. Silva RL, Lopes AH, Guimarães RM, Cunha TM. CXCL1/CXCR2 signaling in pathological pain: role in peripheral and central sensitization. *Neurobiol Dis* 2017; 105: 109–116.
8. Bittar A, Jun J, La JH, Wang J, Leem JW, Chung JM. Reactive oxygen species affect spinal cell type-specific synaptic plasticity in a model of neuropathic pain. *Pain* 2017; 158: 2137–2146.
9. Zhao XY, Zhang QS, Yang J, Sun FJ, Wang DX, Wang CH, He WY. The role of arginine vasopressin in electroacupuncture treatment of primary sciatica in human. *Neuropeptides* 2015; 52: 61–65.
10. Ali U, Apryani E, Wu HY, Mao XF, Liu H, Wang YX. Low frequency electroacupuncture alleviates neuropathic pain by activation of spinal microglial IL-10/ β -endorphin pathway. *Biomed Pharmacother* 2020; 125: 109898.
11. Wang Y, Xue M, Xia Y, Jiang Q, Huang Z, Huang C. Electroacupuncture treatment upregulates α 7nAChR and inhibits JAK2/STAT3 in dorsal root ganglion of rat with spared nerve injury. *J Pain Res* 2019; 12: 1947–1955.
12. Xu Q, Liu T, Chen S, Gao Y, Wang J, Qiao L, Liu J. Correlation between the cumulative analgesic effect of electroacupuncture intervention and synaptic plasticity of hypothalamic paraventricular nucleus neurons in rats with sciatica. *Neural Regen Res* 2013; 8: 218–225.
13. Xu Q, Liu T, Chen S, Gao Y, Wang J, Qiao L, Liu J. The cumulative analgesic effect of repeated electroacupuncture involves synaptic remodeling in the hippocampal CA3 region. *Neural Regen Res* 2012; 7: 1378–1385.
14. Inoue K, Tsuda M. Microglia and neuropathic pain. *Glia* 2009; 57: 1469–1479.
15. Sun S, Cao H, Han M, Li TT, Zhao ZQ, Zhang YQ. Evidence for suppression of electroacupuncture on spinal glial activation and behavioral hypersensitivity in a rat model of monoarthritis. *Brain Res Bull* 2008; 75: 83–93.
16. Shan S, Qi-Liang MY, Hong C, Tingting L, Mei H, Haili P, Yan-Qing W, Zhi-Qi Z, Yu-Qiu Z. Is functional state of spinal microglia involved in the anti-allodynic and anti-hyperalgesic effects of electroacupuncture in rat model of monoarthritis? *Neurobiol Dis* 2007; 26: 558–568.
17. Bernier LP, Ase AR, Séguéla P. P2X receptor channels in chronic pain pathways. *Br J Pharmacol* 2018; 175: 2219–2230.
18. Yang J, Park KS, Yoon JJ, Bae HB, Yoon MH, Choi JI. Anti-allodynic effect of intrathecal processed aconitum jaluense is associated with the inhibition of microglial activation and P2X7 receptor expression in spinal cord. *BMC Complement Altern Med* 2016; 16: 214.
19. Apolloni S, Amadio S, Parisi C, Matteucci A, Potenza RL, Armida M, Popoli P, D'Ambrosi N, Volonté C. Spinal cord pathology is ameliorated by P2X7 antagonism in a SOD1-mutant mouse model of amyotrophic lateral sclerosis. *Dis Model Mech* 2014; 7: 1101–1109.
20. Honore P, Donnelly-Roberts D, Namovic MT, Hsieh G, Zhu CZ, Mikusa JP, Hernandez G, Zhong C, Gauvin DM, Chandran P, Harris R, Medrano AP, Carroll W, Marsh K, Sullivan JP, Faltynek CR, Jarvis MF. A-740003 [N-(1-((cyanoimino)(5-quinolinylamino) methyl)amino)-2,2-dimethylpropyl)-2-(3,4-dimethoxyphenyl)acetamide], a novel and selective P2X7 receptor antagonist, dose-dependently reduces neuropathic pain in the rat. *J Pharmacol Exp Ther* 2006; 319: 1376–1385.
21. Lin JP, Chen CQ, Huang LE, Li NN, Yang Y, Zhu SM, Yao YX. Dexmedetomidine attenuates neuropathic pain by inhibiting P2X7R expression and ERK phosphorylation in rats. *Exp Neurobiol* 2018; 27: 267–276.
22. Kobayashi K, Takahashi E, Miyagawa Y, Yamanaka H, Noguchi K. Induction of the P2X7 receptor in spinal microglia in a neuropathic pain model. *Neurosci Lett* 2011; 504: 57–61.
23. Chessell IP, Hatcher JP, Bountra C, Michel AD, Hughes JP, Green P, Egerton J, Murfin M, Richardson J, Peck WL, Grahames CB, Casula MA, Yiangou Y, Birch R, Anand P, Buell GN. Disruption of the P2X7 purinoceptor gene abolishes chronic inflammatory and neuropathic pain. *Pain* 2005; 114: 386–396.
24. Shen Y, Guan S, Ge H, Xiong W, He L, Liu L, Yin C, Liu H, Li G, Xu C, Xu H, Liu S, Li G, Liang S, Gao Y. Effects of palmitate on rats with comorbidity of diabetic neuropathic pain and depression. *Brain Res Bull* 2018; 139: 56–66.
25. Vadivelu N, Kai A, Maslin B, Kodumudi G, Legler A, Berger JM. Tapentadol extended release in the management of peripheral diabetic neuropathic pain. *Ther Clin Risk Manag* 2015; 11: 95–105.
26. Chu YX, Zhang Y, Zhang YQ, Zhao ZQ. Involvement of microglial P2X7 receptors and downstream signaling pathways in long-term potentiation of spinal nociceptive responses. *Brain Behav Immun* 2010; 24: 1176–1189.
27. Cheung-Flynn J, Alvis BD, Hocking KM, Guth CM, Luo W, McCallister R, Chadalavada K, Polcz M, Komalavilas P, Brophy CM. Normal saline solutions cause endothelial dysfunction through loss of membrane integrity, ATP release, and inflammatory responses mediated by P2X7R/p38 MAPK/MK2 signaling pathways. *PLoS One* 2019; 14: e0220893.

28. Kim EA, Cho CH, Kim J, Hahn HG, Choi SY, Yang SJ, Cho SW. The azetidine derivative, KHG26792 protects against ATP-induced activation of NFAT and MAPK pathways through P2X7 receptor in microglia. *Neurotoxicology* 2015; 51: 198–206.
29. Shiratori M, Tozaki-Saitoh H, Yoshitake M, Tsuda M, Inoue K. P2X7 receptor activation induces CXCL2 production in microglia through NFAT and PKC/MAPK pathways. *J Neurochem* 2010; 114: 810–819.
30. Liang Y, Du JY, Qiu YJ, Fang JF, Liu J, Fang JQ. Electroacupuncture attenuates spinal nerve ligation-induced microglial activation mediated by p38 mitogen-activated protein kinase. *Chin J Integr Med* 2016; 22: 704–713.
31. Deng M, Chen SR, Pan HL. Presynaptic NMDA receptors control nociceptive transmission at the spinal cord level in neuropathic pain. *Cell Mol Life Sci* 2019; 76: 1889–1899.
32. Zimmermann M. Pathobiology of neuropathic pain. *Eur J Pharmacol* 2001; 429: 23–37.
33. Dimitrova A. Introducing a standardized acupuncture protocol for peripheral neuropathy: a case series. *Med Acupunct* 2017; 29: 352–365.
34. Zhao YX, Yao MJ, Liu Q, Xin JJ, Gao JH, Yu XC. Electroacupuncture treatment attenuates Paclitaxel-Induced neuropathic pain in rats via inhibiting spinal glia and the TLR4/NF-kappaB pathway. *J Pain Res* 2020; 13: 239–250.
35. Wan J, Nan S, Liu J, Ding M, Zhu H, Suo C, Wang Z, Hu M, Wang D, Ding Y. Synaptotagmin 1 is involved in neuropathic pain and electroacupuncture-mediated analgesic effect. *Int J Mol Sci* 2020; 21: 968.
36. Zhang H, Sun J, Xin X, Huo Z, Li D. Contralateral electroacupuncture relieves chronic neuropathic pain in rats with spared nerve injury. *Med Sci Monit* 2018; 24: 2970–2974.
37. Hsu HC, Tang NY, Lin YW, Li TC, Liu HJ, Hsieh CL. Effect of electroacupuncture on rats with chronic constriction injury-induced neuropathic pain. *ScientificWorldJournal* 2014; 2014: 129875.
38. Xia YY, Xue M, Wang Y, Huang ZH, Huang C. Electroacupuncture alleviates spared nerve Injury-Induced neuropathic pain and modulates HMGB1/NF- κ B signaling pathway in the spinal cord. *J Pain Res* 2019; 12: 2851–2863.
39. Xing GG, Liu FY, Qu XX, Han JS, Wan Y. Long-term synaptic plasticity in the spinal dorsal horn and its modulation by electroacupuncture in rats with neuropathic pain. *Exp Neurol* 2007; 208: 323–332.
40. Dai WL, Bao YN, Fan JF, Li SS, Zhao WL, Yu BY, Liu JH. Levocorydalmine attenuates microglia activation and neuropathic pain by suppressing ASK1-p38 MAPK/NF- κ B signaling pathways in rat spinal cord. *Reg Anesth Pain Med* 2020; 45: 219–229.
41. Yin Y, Hong J, Pham TL, Shin J, Gwon DH, Kwon HH, Shin N, Shin HJ, Lee SY, Lee WH, Kim DW. Evans blue reduces neuropathic pain behavior by inhibiting spinal ATP release. *Int J Mol Sci* 2019; 20: 4443.
42. Shi Y, Qin W, Nie F, Wen H, Lu K, Cui J. Ulinastatin attenuates neuropathic pain via the ATP/P2Y2 receptor pathway in rat models. *Gene* 2017; 627: 263–270.
43. Wang Z, Mei W, Wang Q, Guo R, Liu P, Wang Y, Zhang Z, Wang L. Erratum to: Role of dehydrocorybulbine in neuropathic pain after spinal cord injury mediated by P2X4 receptor. *Mol Cells* 2019; 42: 376.
44. Xu X, Fu S, Shi X, Liu R. Microglial BDNF, PI3K, and p-ERK in the spinal cord are suppressed by pulsed radio-frequency on dorsal root ganglion to ease SNI-induced neuropathic pain in rats. *Pain Res Manag* 2019; 2019: 5948686.
45. Wang B, Liu S, Fan B, Xu X, Chen Y, Lu R, Xu Z, Liu X. PKM2 is involved in neuropathic pain by regulating ERK and STAT3 activation in rat spinal cord. *J Headache Pain* 2018; 19: 7.
46. Pang J, Hou J, Zhou Z, Ren M, Mo Y, Yang G, Qu Z, Hu Y. Safflower yellow improves synaptic plasticity in APP/PS1 mice by regulating microglia activation phenotypes and BDNF/TrkB/ERK signaling pathway. *Neuromolecular Med* 2020; 22: 341–358.
47. Liu X, Zhao Z, Ji R, Zhu J, Sui QQ, Knight GE, Burnstock G, He C, Yuan H, Xiang Z. Inhibition of P2X7 receptors improves outcomes after traumatic brain injury in rats. *Purinergic Signal* 2017; 13: 529–544.
48. Choi SR, Beitz AJ, Lee JH. Inhibition of cytochrome P450 side-chain cleavage attenuates the development of mechanical allodynia by reducing spinal D-serine production in a murine model of neuropathic pain. *Front Pharmacol* 2019; 10: 1439.
49. Ito G, Suekawa Y, Watanabe M, Takahashi K, Inubushi T, Murasaki K, Hirose N, Hiyama S, Uchida T, Tanne K. P2X7 receptor in the trigeminal sensory nuclear complex contributes to tactile allodynia/hyperalgesia following trigeminal nerve injury. *Eur J Pain* 2013; 17: 185–199.
50. Chen Z, Zhang S, Nie B, Huang J, Han Z, Chen X, Bai X, Ouyang H. Distinct roles of srGAP3-Rac1 in the initiation and maintenance phases of neuropathic pain induced by paclitaxel. *J Physiol* 2020; 598: 2415–2430.
51. Tu WZ, Li SS, Jiang X, Qian XR, Yang GH, Gu PP, Lu B, Jiang SH. Effect of electro-acupuncture on the BDNF-TrkB pathway in the spinal cord of CCI rats. *Int J Mol Med* 2018; 41: 3307–3315.